Generation and Beaming of Early Hot Electrons onto the Capsule in Laser-Driven Ignition Hohlraums

E. L. Dewald, F. Hartemann, P. Michel, J. Milovich, M. Hohenberger, A. Pak, O. L. Landen, L. Divol, H. F. Robey, O. A. Hurricane, T. Döppner, F. Albert, B. Bachmann, N. B. Meezan, A. J. MacKinnon, D. Callahan, and M. J. Edwards

Generation and beaming of early hot electrons onto the capsule in laser-driven ignition hohlraums

E.L. Dewald[1], F. Hartemann[1], P. Michel[1], J. Milovich[1], M. Hohenberger[2], A. Pak[1], O.L. Landen[1], L. Divol[1], H.F. Robey[1], O.A. Hurricane[1], T. Döppner[1], F. Albert[1], B. Bachmann[1], N.B. Meezan[1], A.J. MacKinnon[1], D. Callahan[1] and M.J. Edwards

[1]Lawrence Livermore National Laboratory, P.O. Box 808, Livermore, CA 94550 USA
[2]Laboratory for Laser Energetics, University of Rochester, Rochester, New York 14623, USA

In hohlraums for Inertial Confinement Fusion (ICF) implosions on the National Ignition Facility (NIF), supra-thermal hot electrons, generated by laser plasma instabilities early in the laser pulse ("picket") while blowing down the laser entrance hole (LEH) windows, can preheat the capsule fuel. Hard x-ray imaging of a Bi capsule surrogate and of the hohlraum emissions, in conjunction with the measurement of time resolved Bremsstrahlung spectra allow us to uncover for the first time the directionality of this hot electrons and infer the capsule preheat. Data and Monte Carlo calculations indicate that for most experiments the hot electrons are emitted nearly isotropically from the LEH. However, we have found cases where a significant fraction of the generated electrons are emitted in a collimated beam directly towards the capsule poles, where their local energy deposition is up to 10x higher than the average preheat value and acceptable levels for ICF implosions. The observed "beaming" is consistent with a recently unveiled multi-beam Stimulated Raman Scattering model [P. Michel et al, Phys. Rev. Lett. 115, 055003 (2015)] where laser beams in a cone drive a common plasma wave on axis. Finally, we demonstrate that we can control the amount of generated hot electrons by changing the laser pulse shape and hohlraum plasma.

PACS numbers: 52.57.-z, 52.57.Fg, 52.38.-r

Inertial confinement fusion (ICF) experiments on the National Ignition Facility (NIF) [1] implode and compress a deuterium-tritium (DT) fuel capsule to drive it to ignition and thermonuclear burn [2,3]. In the indirect-drive approach, the ~1 mm-radius capsule is placed inside a high-Z, ~10 mm-long, He-filled, cylindrical cavity (the "hohlraum" [4,5]). NIF's 192 laser beams, grouped in one inner and two outer rings (Fig. 1a insert), hit the interior of the hohlraum wall, converting their energy (up to 2 MJ) to thermal x-rays that ablate the outer layer of the capsule (generally CH), causing the DT fuel to implode. To achieve sufficient compression of the fuel, a carefully tailored sequence of shock waves is launched in the target using a laser pulse that incorporates successive steps in power [6] (Fig. 1a). One main ICF physics challenge that can compromise ignition is supra-thermal hot electrons generated by laser-plasma instabilities that can penetrate through the capsule shell and preheat the fuel, and therefore reducing its compression [2,7]. In particular, at early time in the pulse (the "picket", Fig. 1a), when the fuel is at low temperature, the first shock largely determines the compressed fuel adiabat and the allowable levels of hot electrons are the smallest, i.e. 1000x lower than for the main part of the pulse (the "peak") [6,9]. The acceptable amount of hot electrons is defined as that required to increase the adiabat and lower the no-alpha heating fusion neutron yield by 10% [7,10]. For a typical capsule having a 0.2 mm thick CH ablator, the fuel preheat is caused only by electrons having initial kinetic energies above 170 keV [7]. During the picket, the allowable preheat must be below the DT fuel latent heat of sublimation of 79 J/cc [8] to avoid early fuel decompression (i.e. a raised adiabat) before first shock arrival [6]. For a DT density and mass of 0.25 g/cc and 170 μg, that corresponds to .05 J absorbed in DT and hence ≈ 0.2 J of >170 keV electron energy incident onto the capsule, calculated to lower the neutron yield by 2 kJ [11].

On the NIF, hot electrons are inferred from their Bremsstrahlung emission when stopped in the hohlraum walls using a temporally (~ 0.1 ns) and spectrally resolved (from 20 to 500 keV) hard x-ray spectrometer FFLEX [9,10]. This measurement is not spatially resolved and therefore does not reveal what fraction of the electrons deposit their energy in the fuel capsule. During the picket, they are usually attributed to the two-plasmon decay (TPD) instability near the laser entrance holes (LEH) of the hohlraum where all NIF laser beams from one hemisphere overlap. Indeed, TPD can be collectively driven by multiple beams [12,13], and can only occur near electron densities $n_e \cong n_c/4$ (where n_c is the critical density at the 351 nm laser wavelength), which can be present in the LEH region during the picket as the lasers blow down the high density (1 g/cc), 0.5 um thick plastic window [7,14] that retains the He gas fill (Fig. 1a). Therefore the fraction of hot electrons hitting the capsule was usually estimated by assuming isotropic electron emission from the LEH, as $f_{capsule}=\delta\Omega_{cap}/2\pi \sim 2\%$ (where $\delta\Omega_{cap}$ is the solid angle of the capsule as seen from the LEH).

In this Letter, we present the first measurements of the directionality and non-uniformity of hot electrons in ICF experiments during the picket. These experiments employ hard x-ray imaging of a Bi capsule surrogate and of the hohlraum, time-resolved FFLEX measurements, and are compared to Monte Carlo simulations. While in most cases, the results are consistent with nearly isotropic hot electrons, they have also uncovered a few occurrences where the electrons showed a very strong "beaming" feature, i.e. they were emitted as a collimated beam directly from the LEH towards the capsule. The fraction of hot electrons hitting the capsule $f_{capsule}$ in these cases reached up to 20% (from 2% for an isotropic source). Our results also show that the electron energy deposition in the DT fuel is spatially non-uniform at the capsule, giving more preheat at its poles than at the equator, by a factor ~2 in cases of isotropic emissions and up to a factor ~30 in cases of "beaming". Hot electron beaming appears to be consistent with a multi-beam stimulated Raman scattering process [15], where multiple beams arranged in a cone can collectively drive a common electron plasma wave along the hohlraum axis, accelerating electrons straight

towards the capsule. We finally show that the generated amount of hot electrons can be controlled by shaping the low intensity pre-pulse (the "toe", cf. Fig. 1b), which is usually applied in NIF gas-filled hohlraums to blow down the LEH window to densities below $n_c/4$ (Fig. 1b density map inserts) before launching the higher intensity "picket".

No hot electrons were observed during the 2011-2013 National Ignition Campaign (NIC) experiments [10] that used 1 mg/cc hohlraum fill density [7] and a picket power of 17 TW, preceded by a 0.3 ns long toe with 3 TW power to mitigate TPD. Such electrons were observed first in "High Foot" implosions [11] that employ higher picket power (~ 40 TW, Fig. 1b) to reduce ablation front instabilities [16] compared to NIC. They employ He fill at 1.6 mg/cc density and a 1.2 ns long toe with ~2 TW power. Hot electrons are generated despite 3D hydrodynamic HYDRA simulations [17] which show ~0.10 n_c LEH plasma density on axis during the picket - well below the TPD threshold (Fig. 1b density map inserts). The simulations may not reproduce the experimental conditions well, either due to relatively low resolution in the LEH window or incomplete physics models.

The measured FFLEX spectra, time integrated over the picket (Fig. 1c), have shown hot electron temperatures T_{hot} in the 40-60 keV range. Rather than the total hot electron amount (E_{hot}), throughout this paper, we will refer only to the amount of preheat electrons (energies >170 keV) as a universal preheat metric. Experiments with the same toe pulse and picket power give similar spectra and preheat amount, for a longer picket than the ~300 ps electron burst (Fig. 1b). This suggests that the conditions for generating hot electrons disappear early during the picket.
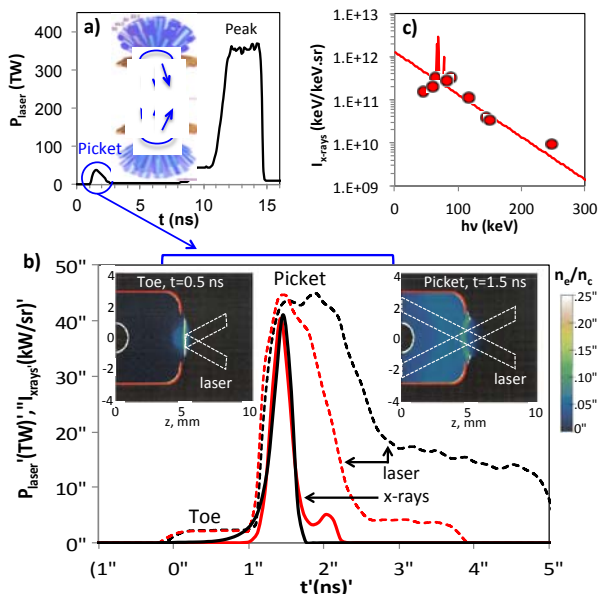
Fig. 1: a) Gas filled hohlraum implosion layout and laser pulse shape, b) zoom-in onto the picket and toe for two different laser pulses (dash red and black) that show similar hot electron levels (> 200 keV x-ray fluence in solid lines) and simulated density maps during toe and picket; c) corresponding time integrated hot electron x-ray spectrum (E_{hot}=15J, T_{hot}=44 keV, 2J in >170 keV electrons).

We have introduced hard x-ray imaging to differentiate the picket hot electrons deposited at the capsule, that can

cause fuel preheat, from those deposited in the hohlraum. In contrast to higher preheat studies during the peak (~500 J vs 2 J) [18], for the picket we replace the CH capsule with a 10 μm thick High-Z Bi shell coated over 25 μm thick CH, and the laser pulses are truncated after ~ 4 ns (Fig. 1b), similar to Reemit experiments [19]. The targets have 3 mm diameter cutouts in the hohlraum that allow for a direct equatorial view of the 2 mm diameter capsule (Fig. 2). Time integrating image plate detectors [20], filtered by 3 mm thick Al, image the target from equatorial and polar directions. Based on the x-ray fluence (Fig. 1c), the pinhole limited imaging resolution was set to 0.5 mm, for 1.6x magnification and a capsule-to-detector distance of 490 mm. When folding in the spectrum, the image plate spectral sensitivity [20] and the x-ray absorption of the Al filter combined with the Bi capsule or the Au hohlraum wall (30 um thick), we find that the centroid photon energy for imaging is 40 keV and has a full width at half maximum (FWHM) of 30 keV.
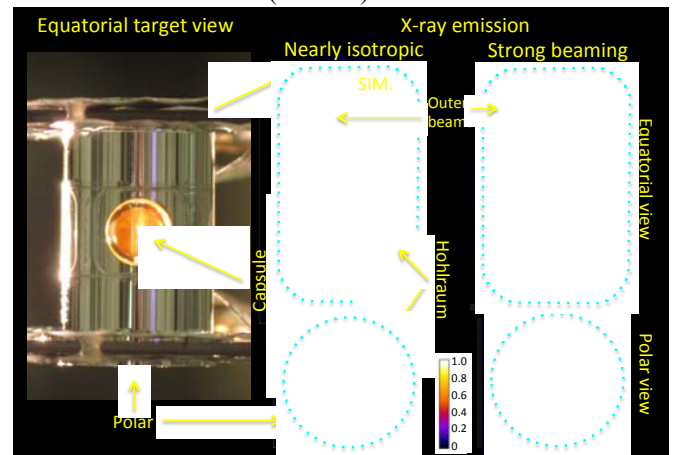
Fig. 2: Target and measured vs simulated (MCNP) 40 keV x-ray emission of hohlraum and capsule for nearly isotropic electrons (1.6 mg/cc fill, 1 TW/1.2 ns long toe, 44 TW picket power, $C_{beaming}$=0.04) and strong electron beaming (0.6 mg/cc fill, 80 TW picket power, 18 TW/0.3 ns long toe, $C_{beaming}$=0.4) experiments.

Hot electron x-ray imaging was used in three types of hohlraum experiments: high gas fill (1.6 mg/cc He, 37-45 TW picket power, 1.2 ns long toe), low and near vacuum gas fill (0.6 mg/cc and 0.03 mg/cc, 80 TW picket power, 0.3 ns long toe). Figure 2 shows that Bi capsule and hohlraum emissions were clearly observed for high and low fill. In all data, the capsule emission is centrally peaked from the polar view and limb brightened from the equator, consistent with pole high electron deposition. We categorize the results as:

- nearly isotropic electrons, with similar capsule and hohlraum x-ray brightness, observed for high gas fill,
- strong electron beaming, for which capsule emission is ~10x brighter than the hohlraum, observed for low fill,
- no hot electrons, observed in near-vacuum (0.03 mg/cc) fill [21], for the same laser pulse as the low fill.

We estimate the fraction of hot electrons stopped in the capsule, $f_{capsule}$, shown in Fig. 3, from the ratio of capsule to hohlraum spatially integrated polar emissions. Predictably, the brighter is the capsule emission with respect to that of the hohlraum, the larger the inferred $f_{capsule}$. Nearly isotropic

electron data shows that, surprisingly, $f_{capsule}$ increases (1.7 to 7%) with the hohlraum preheat rather than being constant at ~2%, as expected for isotropic electrons. The strong beaming experiment gave the highest $f_{capsule}$ of 20%. Monte Carlo N-Particles (MCNP) simulations [22] confirm the spatial correlation between the x-ray emission and the electron energy deposition for both E_{hot} and the preheat electrons. Calculations assume Maxwellian electron distribution with T_{hot} = 40 keV as measured, located on axis, 0.2 mm inwards from the LEH, i.e. the highest density region from HYDRA (Fig. 1b, insert t=1.5 ns). The electron source is assumed to have 0.6 mm radius, given by the FWHM of the overlapped laser beams intensity in that region.
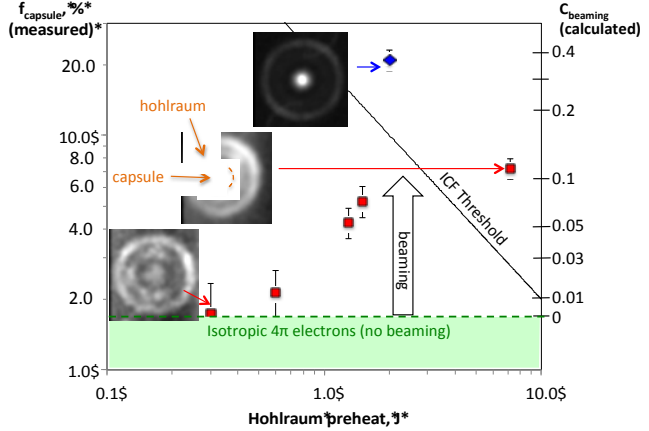
Fig. 3. $f_{capsule}$ vs total hohlraum preheat for nearly isotropic electrons (1.6 mg/cc fill, ~40 TW picket, red points) and strong beaming (0.6 mg/cc fill, 80 TW picket blue point); corresponding polar images clearly show $f_{capsule}$ increases with the capsule-to-hohlraum brightness ratio; inferred $C_{beaming}$ is marked on RHS axis.

We calculate separately electrons that propagate either isotropic in 4π, or beaming straight along the axis, onto the capsule. Isotropic electrons give an $f_{capsule}$ of ~ 1.5%, or 0.75 of the capsule solid angle ($\delta\Omega_{cap}/2\pi$, since backward propagating electrons escape the target). In contrast, for beaming electrons, the calculated $f_{capsule}$ is ~ 50%, consistent with the expected ≈ 50% electron scattering off the Bi shell material [22]. For each experiment, the measured $f_{capsule}$ is matched in calculations by adding a beaming component $C_{beaming}$ to an isotropic source, simply described by:

$$f_{capsule} = f_{capsule}^{beaming} \cdot C_{beaming} + f_{capsule}^{4\pi} \cdot (1 - C_{beaming})$$
$$= 50 \cdot C_{beaming} + 1.5 \cdot (1 - C_{beaming}) \qquad [1],$$

where $C_{beaming}$ is the beaming component relative to the total electron preheat and $f_{capsule}^{beaming,4\pi}$ are the calculated $f_{capsule}$ for beaming and isotropic electrons, respectively. For nearly isotropic electrons experiments, $C_{beaming}$ (marked in Fig. 3 on the RHS axis) increases with the hohlraum preheat from ~ 0 to 0.12 and reaches a significant 0.37 for strong beaming. Simulated images using $C_{beaming}$ from Eq. [1] (Fig. 2) qualitatively agree with the data, except for hohlraum x-ray features from the laser beams that are not included in MCNP. Most of our Fig. 3 data are below the acceptable capsule preheat threshold for ICF [$f_{capsule}\bullet$ (Hohlraum Preheat) < 0.2 J], except for one nearly isotropic and the strong beaming results. Furthermore, while this threshold assumes uniform deposition at the capsule [8], all our results show pole high

electron deposition (Fig. 2), consistent with the electrons being generated at the LEH. We infer the deposition non-uniformity around the capsule from the equatorial limb emission (Fig. 2), normalized to the capsule preheat (Fig. 3). Figure 4 shows the inferred electron deposition vs angle for the strong beaming and one nearly isotropic experiments that yielded similar hohlraum preheat (2 J and 1.3 J, Fig.3), together with matching calculations [$C_{beaming}$ from Eq. (1)] for Bi and fusion (CH+DT) capsules.
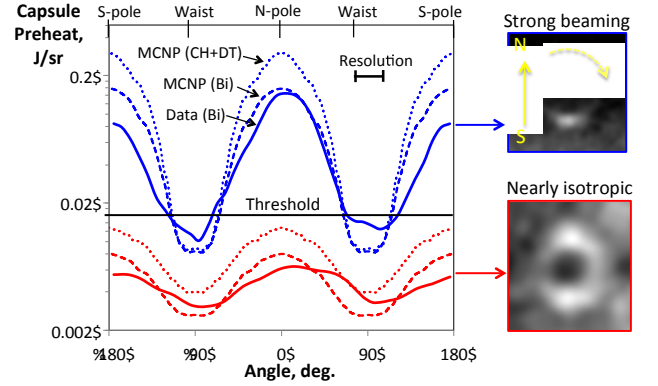
Fig. 4 (a) Equatorial Bi capsule emission and inferred deposition vs angle for strong beaming (blue solid line, $f_{capsule}$=20%) vs nearly isotropic electrons (red solid line, Fig. 3 for $f_{capsule}$=4.2%) with similar hohlraum preheat (2 vs 1.3 J, Fig. 3); calculated deposition for Bi (dashed lines) and fusion capsules (CH+DT, dotted lines).

For nearly isotropic electrons, the measured deposition at the Bi capsule pole is 2.3x higher than on its waist, similar to MCNP calculations that give 3x; the ~25% difference may point towards a larger beaming electron source in the experiment than 0.6 mm radius assumed in MCNP. The calculated deposition asymmetry for the fusion CH capsule is similar to Bi, however, $f_{capsule}$ increases by 33%, due to the electrons not being backscattered in CH (unlike Bi). In contrast, for strong beaming, while the average capsule preheat is only ~2x larger than the ICF threshold (Fig. 3, blue point), the energy deposition at the pole is 14x stronger than at the waist (Fig. 4, blue line) and exceeds locally the threshold by 10x. Bi capsule calculations agree qualitatively with the data, giving 20x pole/waist deposition asymmetry. When Bi is replaced with CH, most of the beaming electrons (97%) are stopped in the capsule poles due to the negligible electron scatter in CH [18]. As a result, for strong beaming ($C_{beaming}$=37%) the calculated $f_{capsule}$ and electron deposition asymmetry double for CH, exceeding the ICF threshold at the poles by ~ 20x (Fig. 4). In conclusion, based only on the FFLEX spectra, for these two experiments (Fig. 4) we would have inferred similar capsule preheat that is ~ 4x below the ICF threshold, assuming isotropic electrons and uniform deposition. However, our x-ray images reveal that for strong beaming the capsule preheat is 30x larger than for weak beaming and exceeds the threshold by 20x. It should be noted that, since the hot electron deposition at the capsule is always pole high, the ICF thresholds, inferred from 1D calculations, are not appropriate. We will improve the estimate of their effect on implosions by adding electron sources similar to our data to 2D hydrodynamic simulations.

Until that work is completed, we adjust the ICF laser pulse to reduce the peak deposition (Fig. 4) below the 1D threshold.

We have only a qualitative picture on the generation of the picket hot electrons. Two possible mechanisms are TPD and a recently proposed multi-beam Stimulated Raman Scattering [24] (MBSRS) model where the electrons are accelerated along the hohlraum axis by an electron plasma wave shared by all laser beams in the LEH region [15]. The TPD instability [12-14], with an exponential gain $G \sim I_{laser} \cdot L_n/T_e$ (I_{laser} - overlapped laser intensity in the plasma region with TPD density scale length L_n and electron temperature T_e) requires $I_{laser} > 10^{14}$ W/cm^2 and $\sim n_c/4$ densities, and the generated hot electrons are isotropic. On the other hand, the MBSRS model suggests an absolute instability for $\sim 0.05\ n_c$ axial density and $I_{laser} > 5 \cdot 10^{13}$ W/cm^2 [15], and is expected to accelerate electrons only in the forward direction, beaming onto the capsule. Both processes are expected to give T_{hot}=30-50 keV that is similar to our data (Fig. 1c) and the laser intensities during the picket are above their thresholds ($7 \cdot 10^{14}$ W/cm^2 for nearly isotropic, $1.5 \cdot 10^{15}$ W/cm^2 for strong beaming). The only difference between TPD and MBSRS in our observables is the electron directionality and hence we use it to infer the possible electron generation mechanisms.
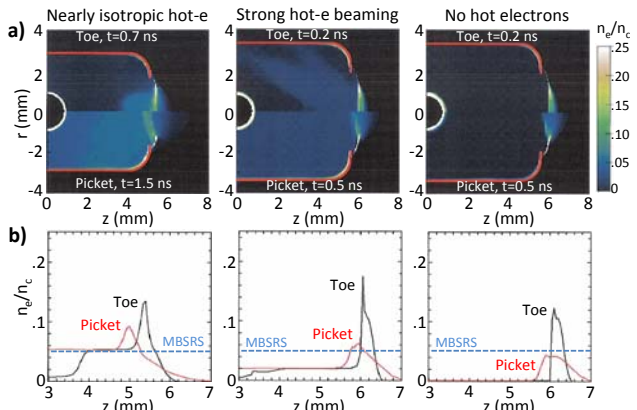
Fig. 5: a) Simulated (3D HYDRA) electron density maps and b) corresponding axial density lineouts during toe and picket (density required for MBSRS shown in blue) averaged over 0.6 mm radius (FWHM of the laser intensity) for nearly isotropic electrons (1.6 mg/cc fill, 44 TW picket power, 1.2 ns toe, Fig. 1b) and strong beaming (0.6 mg/cc fill, 80 TW picket power, 0.3 ns long toe [13]) experiments with similar preheat (Figs. 3,4) and for no hot electron experiment (0.03 mg/cc fill, same laser pulse as strong beaming).

Figure 5 shows density maps and axial density lineouts radially averaged over the FWHM of the overlapped laser beams intensity in the LEH region for the three different cases of hot electron generation, as simulated with HYDRA. For nearly isotropic electrons experiments (Fig. 3), data suggests that hot electrons are mainly generated by TPD, despite simulations showing $0.1n_c << n_c/4$ average density in the picket. For the strong beaming experiment, MBSRS and TPD contribute roughly equally to electron generation. In this case, at 0.6 mg/cc (0.02 n_c) hohlraum fill density, 0.05 n_c MBSRS regions occur (Fig. 5, strong beaming). When the fill is lowered to 0.03 mg/cc, the LEH plasma blows down

more rapidly. Hence, its density in the picket is $< 0.05\ n_c$ (Fig. 5b, RHS) and no electrons are generated, as observed.

Nearly isotropic electrons experiments suggest that while the picket duration does not affect the preheat amount (Fig. 1b), this can be predictably controlled by the toe duration, power, and the picket power, as shown in Fig. 6. The hohlraum preheat decreases with the toe power [$\sim$ exp (-$2P_{Toe}$)] and increases with the picket power [$\sim$ exp ($P_{picket}/4$)]. The picket power scaling is consistent with the TPD gain $\sim I_{laser}$. This also suggests $\sim$200x lower preheat in NIC implosions [10] (17 TW picket) than for 37 TW picket, i.e. well below the FFLEX detection limit (0.05 J), consistent with no hot electrons being measured. An increase in the toe energy may reduce TPD gains by lowering the LEH plasma density and moving it farther from the LEH, towards lower laser intensities (Fig. 1b). The much stronger dependence on toe duration (t_{toe}) than power (P_{Toe}) may be due to the 1D plasma expansion length $\sim \int v_{expansion} dt \sim \int \sqrt{(P_{Toe}t)} dt \sim P_{Toe}^{1/2} \cdot t_{toe}^{3/2}$. Note that TPD and MBSRS gains are only threshold values and cannot explain these preheat scalings.
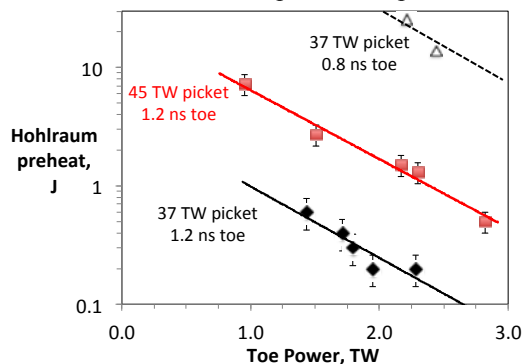
Fig. 6: Measured preheat for nearly isotropic electrons (1.6 mg/cc fill) vs toe power for picket powers of 45 TW/1.2 ns toe (red) and 37 TW (black: diamonds for 1.2 ns toe, triangles for 0.8 ns toe).

In summary, hot electrons were observed for the first time during the picket in ICF gas filled hohlraums, when the laser beams burn through the LEH windows. For 1.6 mg/cc He hohlraum fill, most of the generated hot electrons are isotropic, with $< \sim 0.1$ of the total electrons beaming towards the capsule. In contrast, for 0.6 mg/cc fill, a significant ~ 0.4 fraction of the generated electrons are beaming directly onto the capsule. For this case the total electron deposition in a Bi capsule surrogate is $\sim$10x higher than for isotropic electrons. Since they are generated at the LEH, all experiments show a pole high electron deposition at the capsule, that is much more asymmetric for strong beaming, further increasing the local preheat by 10x above its average. The amount of generated hot electrons can be predictably controlled by the laser toe power and duration and by the picket power.

[1] G.H. Miller, E.I. Moses, C.R. Wuest, Nucl. Fusion **44,** 228 (2004).
[2] J.D. Lindl, P. Amendt, R.L. Berger, S.G. Glendinning, S.H. Glenzer, S.W. Haan, R.L. Kauffman, O.L. Landen, *Phys. Plasmas* **11**, 339 (2004).

[3] O.L. Landen, T.R. Boehly, D.K. Bradley, D.G. Braun, D.A. Callahan, P.M. Celliers, G.W. Collins, E.L. Dewald, L. Divol, S.H. Glenzer, A. Hamza, D.G. Hicks, N. Hoffman, N. Izumi, O.S. Jones, R.K. Kirkwood, G.A. Kyrala, P. Michel, J. Milovich, D.H. Munro, A. Nikroo, R.E. Olson, H.F. Robey, B.K. Spears, C.A. Thomas, S.V. Weber, D.C. Wilson, M.M. Marinak, L.J. Suter, B.A. Hammel, D.D. Meyerhofer, J. Atherton, J. Edwards, S.W. Haan, J.D. Lindl, B.J. MacGowan, E. I. Moses, *Phys. Plasmas* **17**, 056301 (2010).

[4] G.D. Tsakiris, J. Massen, R. Sigel, F. Lavarenne, R. Fedosejevs, J. Meyer-ter-Vehn, K. Eidmann, S. Witkowski, H. Nishimura, Y. Kato, H. Takabe, T. Endo, K. Kondo, H. Shiraga, S. Sakabe, T. Jitsuno, M. Takagi, C. Yamanaka, S. Nakai, *Phys. Rev. A* **42**, 6188 (1990); W.A. Stygar, R.E. Olson, R.B. Spielman, R.J. Leeper, *Phys. Rev. E* **64**, 026410 (2001).

[5] F. Phillippe, A. Casner, T. Caillaud, O. Landoas, M.C. Monteil, S. Liberatore, H.S. Park, P. Amendt, H. Robey, C. Sorce, C.K. Li, F. Seguin, M. Rosenberg, R. Petrasso, V. Glebov, C. Stoeckl, *Phys. Rev. Lett.* **104**, 035004 (2010).

[6] H.F. Robey, T.R. Boehly, P.M. Celliers, J.H. Eggert et al, *Phys. Plasmas* **19,** 042706 (2012).

[7] S.W. Haan *et al., Phys. Plasmas* **18**, 051001 (2011).

[8] P. C. Souers, *Hydrogen Properties for Fusion Energy*, University of California Press, Berkeley, 1986.

[9] E.L. Dewald, C. Thomas, S. Hunter, L. Divol, N. Meezan, S.H. Glenzer, L.J. Suter, E. Bond, J.L. Kline, J. Celeste, D. Bradley, P. Bell, R.L. Kauffman, J. Kilkenny, O.L. Landen, *Rev. Sci. Instrum.* **81**, 10D938 (2010); M. Hohenberger, F. Albert, N.E. Palmer, J.J. Lee, T. Döppner, L. Divol, E.L. Dewald, B. Bachmann, A.G. MacPhee, G. LaCaille, D.K. Bradley, C. Stoeckl, *Rev. Sci. Instrum.* **85**, 11D501 (2014).

[10] J.D. Lindl et al, *Phys. Plasmas* **21**, 020501 (2014).

[11] O.A. Hurricane, D.A. Callahan, D.T. Casey, P.M. Celliers, C. Cerjan, E.L. Dewald, T.R. Dittrich, T. Döppner, D.E. Hinkel, L.F. Berzak Hopkins, J.L. Kline, S. Le Pape, T. Ma, A.G. MacPhee, J.L. Milovich, A. Pak, H.-S. Park, P.K. Patel, B.A. Remington, J.D. Salmonson, P.T. Springer, R. Tommasini, *Nature* **506**, 343 (2014).

[12] C. Stoeckl, R.E. Bahr, B. Yaakobi, W. Seka, S.P. Regan, R. Craxton, J. Delettrez, R. Short, J. Myatt, A.V. Maximov, H. Baldis, *Phys. Rev. Lett.* **90**, 235002 (2003).

[13] D.T. Michel, A.V. Maximov, R.W. Short, S.X. Hu, J.F. Myatt, W. Seka, A. A. Solodov, B. Yaakobi, D.H. Froula, *Phys. Rev. Lett.* **109**, 155007 (2012).

[14] S.P. Regan et al, *Phys. Plasmas* **17**, 020703 (2010).

[15] P. Michel, L. Divol, E.L. Dewald, J.L. Milovich, M. Hohenberger, O.S. Jones et al, L. Berzak Hopkins, R.L. Berger, W.L. Kruer, J.D. Moody, *Phys. Rev. Lett.* **115,** 055003 (2015).

[16] D. Casey et al, *Phys. Rev. E* **90**, 011102 (2014).

[17] M.M. Marinak, G. D. Kerbel, N. A. Gentile, T.R. Dittrich, and S. W. Haan, *Phys. Plasmas* 8, 2275 (2001).

[18] T. Do ppner, C.A. Thomas, L. Divol, E.L. Dewald, et al, *Phys. Rev. Lett.* **108***,* 135006 (2012).

[19] E.L. Dewald, J. L. Milovich, P. Michel, et al, *Phys. Rev. Lett.* **111**, 235001 (2013).

[20] A.L. Meadowcroft, C.D. Bentley, E.N. Stott, *Rev. Sci. Instrum.* **79**, 113102 (2008).

[21] L. Berzak Hopkins, N. Meezan, S. Le Pape, L. Divol, A. Mackinnon, D. D. Ho, M. Hohenberger, O. S. Jones, G. Kyrala, J. L. Milovich et al., *Phys. Rev. Lett.* **114**, 175001 (2015).

[22] T. Goorley, et al., *Nucl. Technol.* **180**, 298 (2012).

[23] T. Tabata, R. Ito, S. Okabe, *Nucl. Instrum. Meth.* **94**, 509 (1971).

[24] B.B. Afeyan and E. A. Williams, *Phys. Rev. Lett.* **75,** 4218 (1995).